The influences of size effect and stress condition on fracture behavior and ductile fracture occurrence in micro-scaled plastic deformation

J.L. Wang, M.W. Fu[a,b *], S.Q. Shi

[a]Department of Mechanical Engineering, The Hong Kong Polytechnic University, Hung Hom, Kowloon, Hong Kong

*Tel: 852-27665527, Email: mmmwfu@polyu.edu.hk

Abstract

In macro-scaled plastic deformation processes, ductile fracture has been extensively investigated in the field of formation mechanism, deformation mechanics, influencing factors and fracture criteria. However, in micro-scaled plastic deformation, the material deformation and fracture behaviors are great different from those in macro-scale due to the existence of size effects, which lead to the change of mechanical behaviour of materials. In order to explore the simultaneous interaction of size effect and stress condition on material fracture behaviour in meso/micro-scaled plastic deformation, multi-scaled tensile and compression tests of pure copper with various geometrical sizes and microstructures were conducted. The experiment results expose that microvoids exist in compressed samples due to localization of shear band instead of macro fracture. Furthermore, the FE simulation is conducted by using the size dependent surface layer model to study the interaction of size effect and stress condition on material fracture behavior in multi-scaled deformation. It is found that the stress triaxiality (T) generally increases with the ratio of surface grains η in compression statement. Fracture strain and fracture energy with positive T are much smaller than that with negative T regardless of geometrical and grain sizes. This research deeply investigates the fracture behavior in micro-scaled plastic deformation.

Keywords: Size effect, Stress condition, Ductile fracture, Micro-scaled plastic deformation

1. Introduction

With the increasingly demand for product miniaturization from microelectronics, biomedicine, consumer electronics, and many other industrial clusters, how to make micro-scaled parts and components has attracted many attentions in academia and industry. Microforming technology is thus developed and microforming technology has emerged as a promising micromanufacturing process due to its high production, minimized material loss**,** excellent mechanical properties and close tolerance [1, 2]. Although this micromanufatcuring has promising potential in a large-scale of industrial applications, there is a lack of systematic theory and knowledge to support the application of microforming technology in micro-scaled part design, microforming process determination and tooling design. There is also difficulty in leveraging the existing and well-established forming knowledge in macro(m)-scale to micro(μ)-scale as the existence of size effect in the latter actually hinders this type of knowledge transfer and the systematic knowledge verification in μ-scale is critical. Therefore, the material deformation behavior affected by size effects including ductile fracture (DF), mechanism of fracture and damage accumulation should be further investigated and analyzed in micro scaled domain.

In metal forming, many efforts have been made to improve the formability of materials, which is greatly affected by DF. Therefore, an accurate ductile fracture criterion (DFC) for prediction and analysis of DF is imperatively needed in design of metal forming products and forming process. Various physical experiments and microscopic observation found that macro fracture behavior resulted from micro-void and shear bands, which lead to the presence of several micro-mechanically motivated DFCs [3-5]. In consideration of interaction of constitutive model and material damage model, these criteria are divided into uncoupled and coupled categories. For uncoupled DFCs, damage value is calculated empirically considering

state variables such as equivalent plastic stress and strain, hydrostatic stress, and stress triaxiality (T) [6, 7]. The common expression is formulated in Eq. (1).

$$\int_0^{\varepsilon_f} f\left(\sigma,\varepsilon\right) d\varepsilon = C_c \tag{1}$$

Where ε_f is fracture strain, σ is effective stress, ε is effective strain, C_c is critical fracture criteria value.

While damage reaches a critical value, fracture is considered to occur. The state variables involved in an equation directly or indirectly indicate the physical essence of macroscopic DF behavior. In the traditional metal plasticity theory, the hydrostatic pressure and third deviatoric stress have a negligible influence on the flow stress, however, Bai et al. [8] concluded that both state variables should be taken into account of the constitutive equation of materials and proposed a general form of asymmetric metal plasticity, including both the pressure sensitivity and the Lode parameters, furthermore, discussed a calibration method. Liu and Fu [9] stated a modified DFC based on the Ayada criterion, which considers influences of T and the equivalent plastic strain on DF behavior. Hamblia and Reszka [10] suggested a computation methodology using inverse technique to simulate circular blanking and identify the critical values of DFCs and predicted crack initiation and propagation generated by shearing mechanisms. Li et al. [11] conducted tensile and compression tests of Al-alloy 6061 (T6) with different sample shapes and dimensions to get varying stress and strain states and DF modes, and studied several uncoupled and coupled DFCs, and further studied their reliability in DF prediction using finite element (FE) simulation.

However, abovementioned efforts are mainly focused on macro-forming process. As for microforming process, DF behavior are different from that in m-scale, and thus needs systematic investigation. Considering the size effects Ran et al. [12] proposed a size effect-based surface layer model(SLM), which was tested and verified by the micro scale flanged upsetting experiments, to predict the DF initiation in the μ-scaled plastic deformation process and concluded that ductile fracture in μ-scaled deformation is difficult to occur because of the size effects. Furthermore, Ran and Fu [13] presented a hybrid model of multiphase alloys, which identifies the contribution of each phase to the property of material and utilizes damage energy to predict the DF in μ-scaled deformation. Meng and Fu [14] conducted uniaxial tensile tests using pure copper sheets with different thickness(t) and grain size(d) and revealed that the flow stress, fracture strain, and the amount of microvoids on fracture surface are getting smaller with the decreasing ratio of t to d.

As mentioned above, there is still a lack of deeply investigation of DF and its behavior in μ-scaled plastic deformation. In μ-scaled domain, the major influencing factors of DF identified in m-scaled domain may include invariant tensors, hydrostatic stress, and stress triaxiality (T) still needs in-depth investigation. The objective of this research to study the interaction of size effect and stress condition on material fracture behavior in multi-scaled deformation processes. So, the SLM is used to describe the size effects of materials as shown in Fig.1 and multi-scaled uniaxial tensile and compression test with different geometrical sizes and microstructures are conducted to get true stress-strain relationships and different stress triaxiality (T). And furthermore numerical simulations considering size effect are performed and the results are verified by experiment results. Finally, the influence of size effects and stress triaxiality (T) on fracture strain and energy will be in-depth explored.

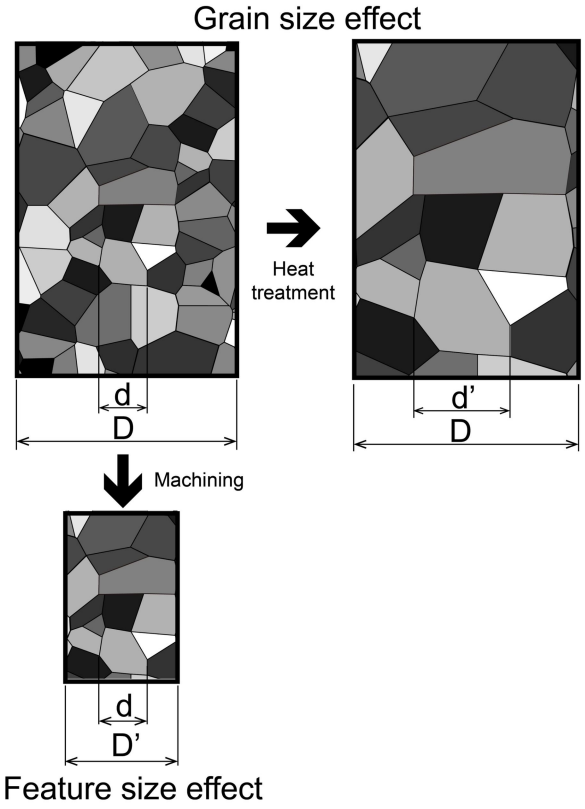

Fig. 1. Graphic explanation of feature and grain size effects.

2. Research methodology

2.1. Research procedure

The flowchart of research is presented in Fig. 2. To describe the meso/μ-scale flow stress, the SLM [15] was employed and Small meso-scale compression tests and uniaxial tensile test were conducted to calculate the stress-strain. The SLM was then used in the FE simulations to simulate DF behavior. Moreover, uniaxial tensile tests with different thickness(t) and grain size(d) and large meso/μ-scale compression tests were carried out. The strain–stress relationship of tensile and compression tests was obtained and compared with the simulation results to identify the damage and size-related parameters. The deep drawing experiments using pure cooper sheets with different grain sizes were then conducted and compared with predicted simulation results.

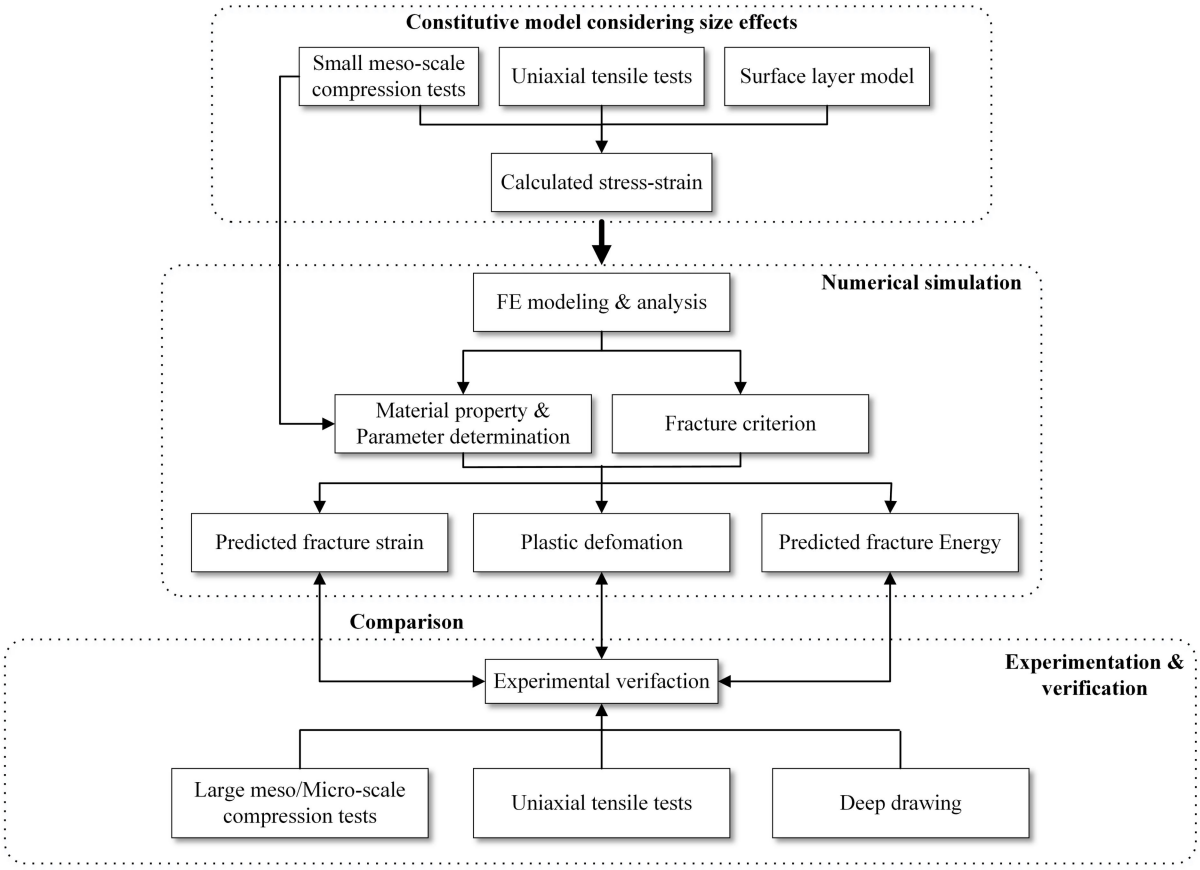

Fig. 2. Flowchart of research procedure.

2.2. SLM considering size effects

Based on the SLM, the polycrystalline material is considered to be comprised of surface and inner portions as shown in Fig. 3. Consequently, the flow stress of the material consists of two types of flow stresses: the flow stress of inner grains and surface grains. The surface grains are less restricted than the inner grains, which results in an easy sliding and rotation deformation. The surface grains thus have lower flow stress than the inner ones. Based on the SLM, the flow stress can be expressed as:

$$\begin{cases} \sigma = \eta\sigma_s + (1-\eta)\sigma_i \\ \eta = \dfrac{N_s}{N} \end{cases} \tag{2}$$

In Eq. (2), σ and N indicate the flow stress and entire grain number of material. σ_s and N_s represent the flow stress and the number of surface grains. σ_i is the flow stress of inner grains. In m-forming, the ratio η of surface grains is negligible and contribution of the surface grains to material property can be neglected. However, when the sample is scaled down to meso- or μ-scale, η increases and the influence of surface grains are getting more important in plastic deformation process.

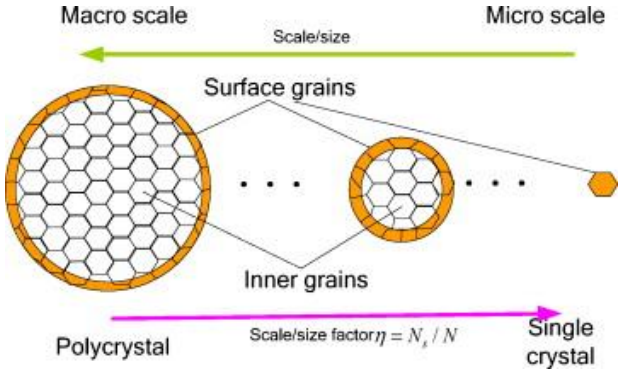

Fig. 3. Distribution of grains in a workpiece section with the decreasing geometrical size[16].

Based on the SLM, Lai et al. [17] presented a hybrid constitutive model to represent the material flow stress-strain relationship. In this model, the property of surface grains is regarded as similar to single crystal while the inner bulk is treated as polycrystal. According to crystal plastic theory and Hall-Petch equation [18, 19] the stress of the surface and inner grains can be described as:

$$\begin{cases} \sigma_s(\varepsilon) = m\tau_R(\varepsilon) \\ \sigma_i(\varepsilon) = M\tau_R(\varepsilon) + \dfrac{k(\varepsilon)}{\sqrt{d}} \end{cases} \tag{3}$$

In Eq. (3), d is the grain size; m and M are the orientation factors of single crystal and polycrystal, respectively; $\tau_R(\varepsilon)$ is critical resolved shear stress of single crystal, and $k(\varepsilon)$ is locally stress required to pass polycrystal grain boundaries. Combining Eqs. (1) and (3), the flow stress expression of meso/μ-scale material is written as:

$$\sigma(\varepsilon)=\eta m\tau_R(\varepsilon)+(1-\eta)\left(M\tau_R(\varepsilon)+\frac{k(\varepsilon)}{\sqrt{d}}\right) \tag{4}$$

When size factor η = 0, the $\sigma(\varepsilon)$ represents an polycrystal material model. When η = 1, the $\sigma(\varepsilon)$ is a single crystal material model. According to Eq. (4), the mixed model can be separated into two parts: size dependent part, i.e. σ_{dep} and size independent part, σ_{ind}. And the form of mixed model can be written as [16]:

$$\begin{cases}\sigma(\varepsilon)=\sigma_{ind}+\sigma_{dep}\\ \sigma_{ind}=M\tau_R(\varepsilon)+\dfrac{k(\varepsilon)}{\sqrt{d}}\\ \sigma_{dep}=\eta\left(m\tau_R(\varepsilon)-M\tau_R(\varepsilon)-\dfrac{k(\varepsilon)}{\sqrt{d}}\right)\end{cases} \tag{5}$$

In Eq. (5), σ_{dep} and σ_{ind} indicate the size dependent and independent flow stress, respectively.

2.3. Model calculation in meso/μ-scale bulk forming process

The surface and inner grains of billet in meso/μ-scale bulk forming process is shown in Fig.4. (a). The feature size, i.e. diameter of the billet, is D and the grain size is d. The billet is cylinder and the grain is considered as sphere. The proportion of surface grains can be calculated by volume ratio as follows:

$$\begin{cases}\eta=\dfrac{N_s}{N}=\dfrac{\dfrac{\pi D^2H}{4}-\left[\dfrac{\pi}{4}(D-2d)^2(H-2d)\right]}{\dfrac{\pi D^2H}{4}}=1-\dfrac{\left[(D-2d)^2(H-2d)\right]}{D^2H} & D\neq d\\ \eta=1 & D=d\end{cases} \tag{6}$$

2.4. Model calculation in meso/μ-scale sheet forming process

Fig. 4. (b) shows the schematic cross section of the sheet in meso/μ-scale. The proportion of surface grains in the cross section can be calculated as:

$$\eta = \frac{N_s}{N} = \frac{wt - \left[(w-2d)(t-2d)\right]}{wt} = \frac{2d}{t} + \frac{2d}{w} - \frac{4d^2}{wt} \tag{7}$$

Where w and t are the width and thickness of sheet, respectively. In meso/μ-forming process, w is usually much larger than t and d, thus $2d/w \approx 0$, $4d^2/wt \approx 0$, so Eq. (7) can be simplified as:

$$\eta = \frac{2d}{t} \tag{8}$$

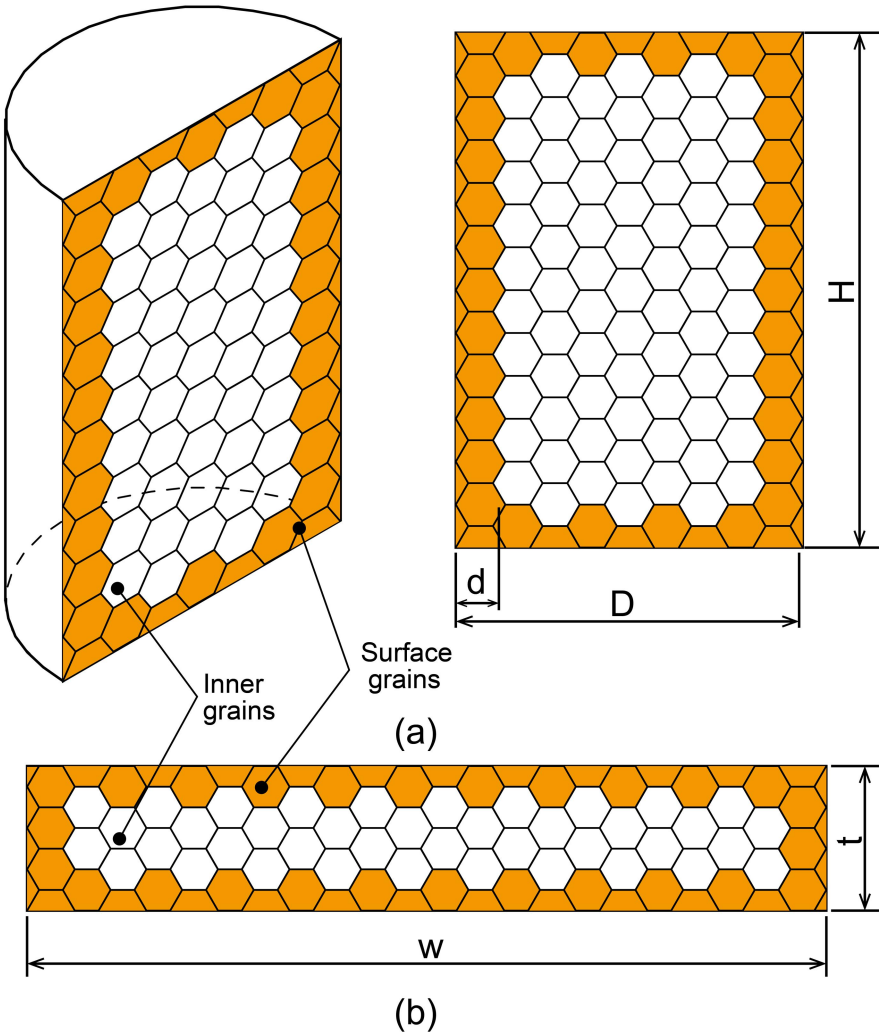

Fig. 4. The surface layer model of the meso/micro-scale samples. (a). Billet sample (b). Sheet sample.

3. Experiments

3.1. Specimens preparation

Three types of pure copper billets with the dimensions of Ø 2.6×3, Ø 1.3×1.5 and Ø 0.65×0.75 mm represent large meso-, small meso-, and micro-scale, respectively, which were used for compression test, while, pure copper sheet with the thickness of 0.2, 0.4, 0.6 mm was used for tensile test. These samples were annealed at different temperatures and dwelling times, viz., 500 °C for 1 h, 600 °C for 2 h and 750 °C for 3 h in vacuum environment to get different grain sizes, as listed in Table 1. Fig. 5 shows the microstructures of material.

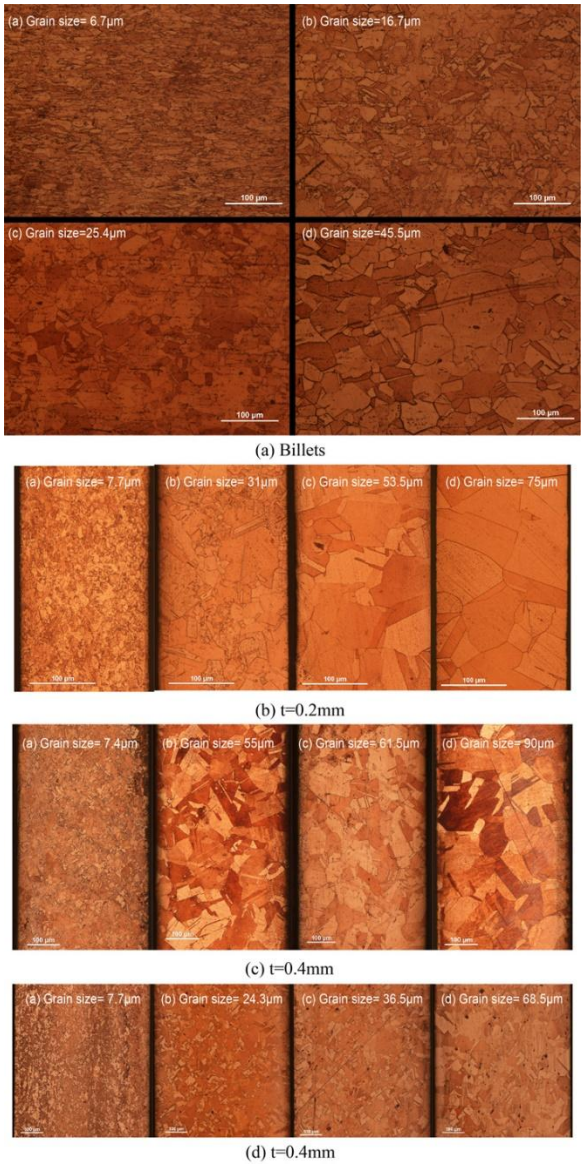

Fig. 5. Microstructures of the pure copper. (a). As-received, and annealed at (b)500 ºC, (c). 600 ºC, (d). 750 ºC.

Table. 1 Annealing parameters.

Samples	Temperature (ºC)	Dwelling hour (h)	Average grain size (μm)
Billet	As-received	N/A	6.7
	500	1	16.7
	600	2	25.4
	750	3	45.5
t=0.2	As-received	N/A	7.7
	500	1	31
	600	2	53.5
	750	3	75
t=0.4	As-received	N/A	7.4

	500	1	55
	600	2	61.5
	750	3	90
	As-received	N/A	7.7
t=0.6	500	1	24.3
	600	2	36.5
	750	3	68.5

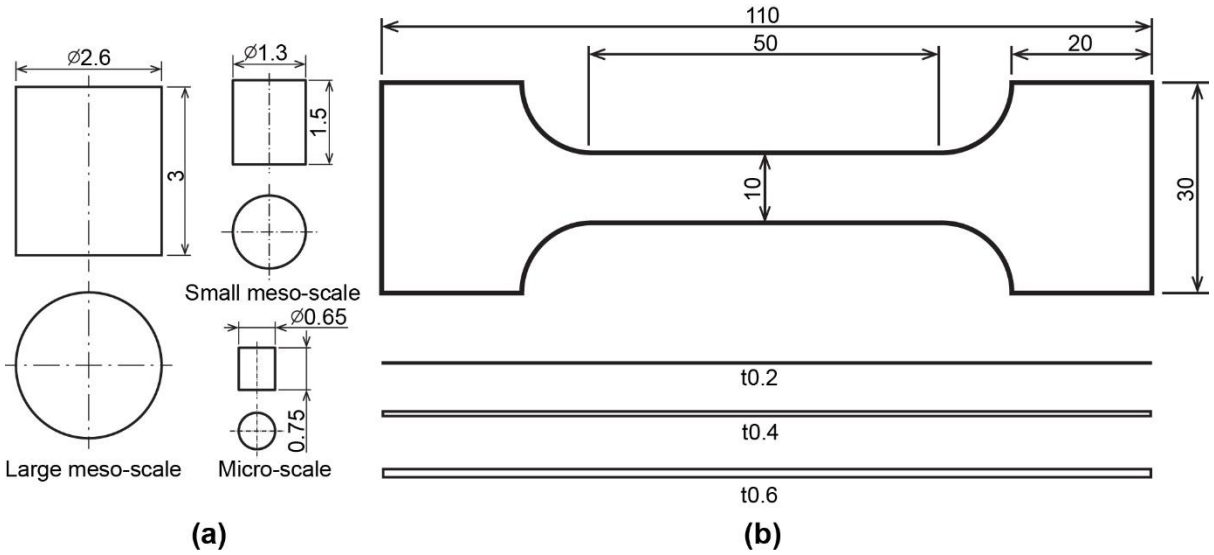

Fig. 6. Experimental samples. (a) Billets in different feature size, (b) Sheets in different thickness.

3.2. Compression tests

The stress–strain relationship of pure copper was obtained through large meso-, small meso-, and μ-scale compression tests, and the dimensions are Ø 2.6×3, Ø 1.3×1.5 and Ø 0.65×0.75 mm, respectively, as shown in Fig.6 (a). All samples were lubricated with machine oil to minimize frictional effect and compressed on the MTS experiment platform with a load cell of 30 KN. Each type of test was repeated three times to eliminate testing error. The crosshead velocity of the testing platform was set to be 0.04, 0.02 and 0.01 mm/s for large meso-, small meso- and μ-scaled billets, respectively. All the samples were compressed by 75% of the corresponding height at room temperature and then these samples were inspected by scanning electron microscope. Subsequently, the compressed specimens were cut along the symmetry

plane to examine the inner microstructure. The loading and extension data were collected via a built-in data acquisition system. The true stress–strain curves for the small meso-scaled billets with different d are presented in Fig. 7. It can be seen that the as-received sample (d=6.7μm) shows a greatly high yield stress and strain softening caused by stress concentration and undiscovered flaw in the previous forming process.

Flow stress is significantly reduced with the increase of grain size. The SLM proposed by Lai et al. [17] was used to explain the size effect on flow stress. Based on the model, m and M in Eq. (5) were set to be 2 and 3.06 respectively [20, 21]. $\tau_R(\varepsilon)$ and $k(\varepsilon)$ are fitted to the exponential function according to the least square method:

$$\begin{cases} \tau_R(\varepsilon) = k_1 \varepsilon^{n_1} \\ k(\varepsilon) = k_2 \varepsilon^{n_2} \end{cases} \tag{9}$$

The fitted results and flow stresses of internal grains $\sigma_i(\varepsilon)$ and surface grains $\sigma_s(\varepsilon)$ are shown in Fig.8. The fitted parameters are shown in Table. 2. The final model is:

$$\begin{cases} \sigma_{ind} = M\tau_R(\varepsilon) + \dfrac{k(\varepsilon)}{\sqrt{d}} = 315.5\varepsilon^{0.45} + 20.3\varepsilon^{0.198} d^{-\frac{1}{2}} \\ \sigma_{dep} = \eta\left(m\tau_R(\varepsilon) - M\tau_R(\varepsilon) - \dfrac{k(\varepsilon)}{\sqrt{d}} \right) = \eta\left(206.2\varepsilon^{0.45} - 315.5\varepsilon^{0.45} - 20.3\varepsilon^{0.198} d^{-\frac{1}{2}} \right) \\ \sigma(\varepsilon) = \sigma_{ind} + \sigma_{dep} = (1-\eta)315.5\varepsilon^{0.45} + \eta 206.2\varepsilon^{0.45} + (1-\eta)20.3\varepsilon^{0.198} d^{-\frac{1}{2}} \end{cases} \tag{10}$$

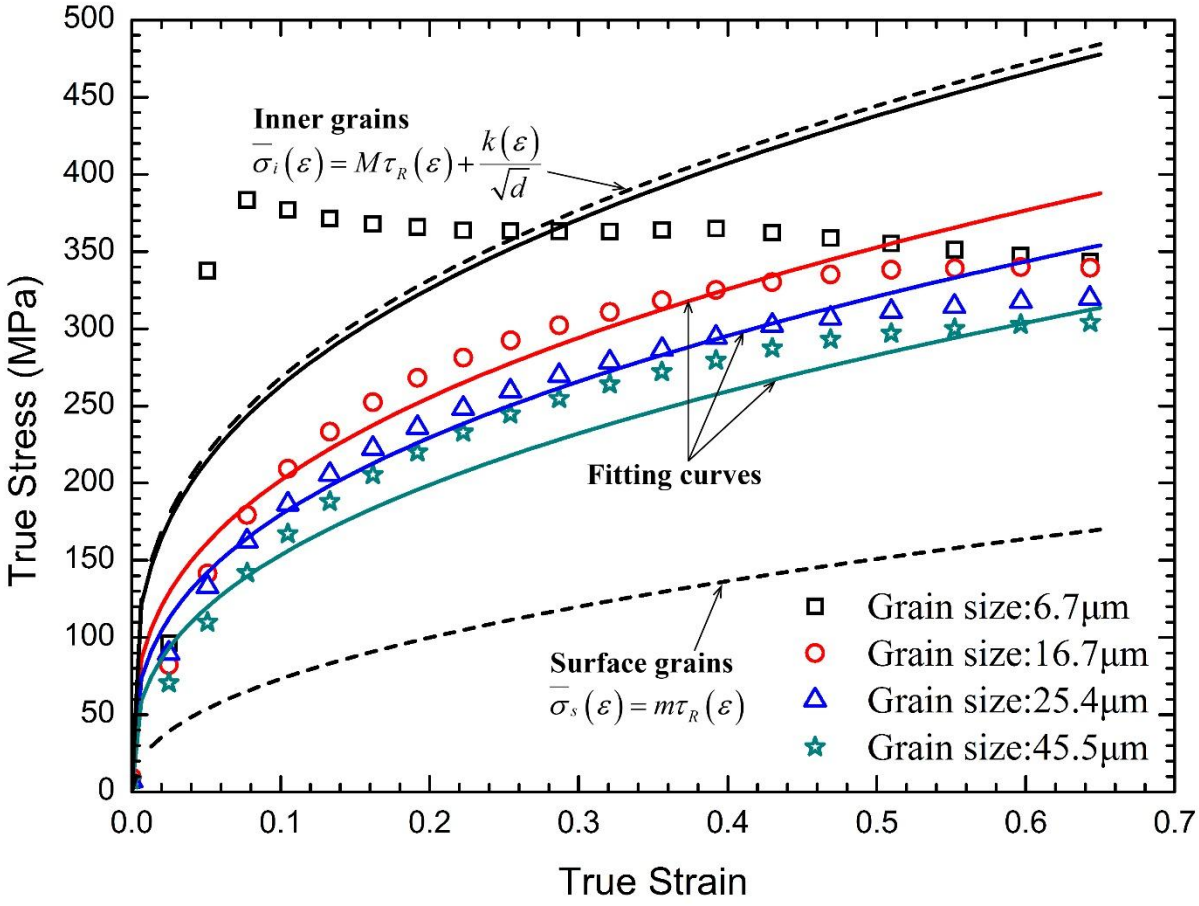

Fig. 7. Flow stress–strain curves of the small meso-scale billet.

Table. 2 The fitted parameters of SLM.

Parameters	Small meso-scale	t=0.4 mm
k^1	103.1	223.6
n^1	0.45	0.74
k^2	20.3	22.5
n^2	0.198	0.165

3.3. Uniaxial tensile test

Sheets with the thickness 0.2, 0.4, and 0.6 mm, as shown in Fig. 6, were used for uniaxial tensile tests conducted in an MTS platform. The flow stress–strain curves were obtained as shown in Fig. 8. The elongation of the specimens was measured by an extensometer with the gauge length of 25 mm until fracture under a constant strain rate of 0.004 mm/s. For each specimen with the same average *d* and *t*, the uniaxial tensile tests were conducted five times

to eliminate testing error. After the tests, the fracture surfaces of specimens were observed via SEM. Furtherly, the cross-sectional photograph of fracture surfaces along the thickness direction were also recorded.

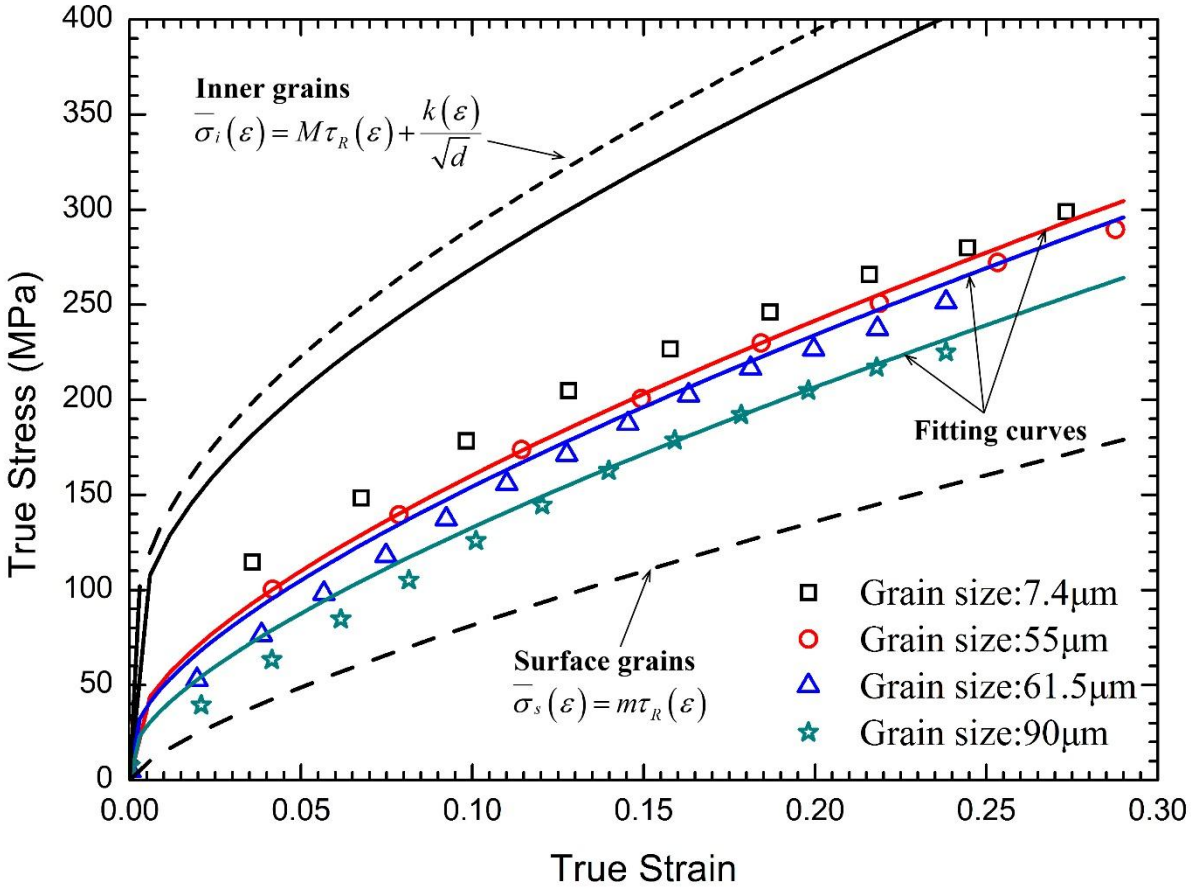

Fig. 8. Flow stress-strain curves of the sheet with t= 0.4 mm.

It is found that the as-received material with the d=7.4μm shows a greatly high flow stress caused by the residual stress in the foregoing rolling process. $\tau_R(\varepsilon)$ and $k(\varepsilon)$ are fitted to exponential function according to the least square method:

$$\begin{cases} \tau_R(\varepsilon) = k_1' \varepsilon^{n_1'} \\ k(\varepsilon) = k_2' \varepsilon^{n_2'} \end{cases} \tag{11}$$

The fitted results and flow stresses of internal grains $\overline{\sigma}_i(\varepsilon)$ and surface grains $\overline{\sigma}_s(\varepsilon)$ are shown in Fig.8. The fitted parameters are shown in Table. 2.

The final model as follow:

$$\begin{cases} \sigma_{ind} = M\tau_R(\varepsilon) + \dfrac{k(\varepsilon)}{\sqrt{d}} = 684.2\varepsilon^{0.74} + 22.5\varepsilon^{0.165} d^{-\frac{1}{2}} \\ \sigma_{dep} = \eta\left(m\tau_R(\varepsilon) - M\tau_R(\varepsilon) - \dfrac{k(\varepsilon)}{\sqrt{d}} \right) = \eta\left(447.2\varepsilon^{0.74} - 684.2\varepsilon^{0.74} - 22.5\varepsilon^{0.165} d^{-\frac{1}{2}} \right) \\ \sigma(\varepsilon) = \sigma_{ind} + \sigma_{dep} = (1-\eta)684.2\varepsilon^{0.74} + \eta 447.2\varepsilon^{0.74} + (1-\eta)22.5\varepsilon^{0.165} d^{-\frac{1}{2}} \end{cases} \quad (12)$$

4. Result and analysis

4.1. Experimental results and discussion

Fig. 9 shows the circumferential surface deformation behaviors of different geometrical sizes specimens with different *d*. The circumferential surface grains of the specimen distributed along shear bond with an angle of about 45° to the compression direction indicated by arrows in Fig. 9. For C1: *d*=6.7μm (as-received) the surface grains are uniformly distributed in deformation process but the deformation localization is gradually severe for the specimen with the *d* from 16.7 to 45.5μm. For the C4: *d*=45.5μm the deformation is also highly inhomogeneous. This can be explained by the SLM. When the ratio of feature size to grain size is excessive large, surface grains can be negligible, and thus the deformation of specimens is similar to the polycrystal materials. With the decrease of η, the influence of surface layer is increasingly significant. The variations of grain orientation and properties increase and lead to uneven grains distribution.

Furthermore, micro-cracks are observed on the circumferential surfaces of compressed specimens. On account of excellent ductility of pure copper there are not obvious

macroscopic cracks on the surface. With the increase of grain size the slip band is greatly affected by single grain orientation and property. For C4 in Fig.9 the slip band is combined with grain boundary and cracks are also located at grain boundaries. In order to deeply investigate the inner microstructure the compressed samples were cut along the symmetry plane.

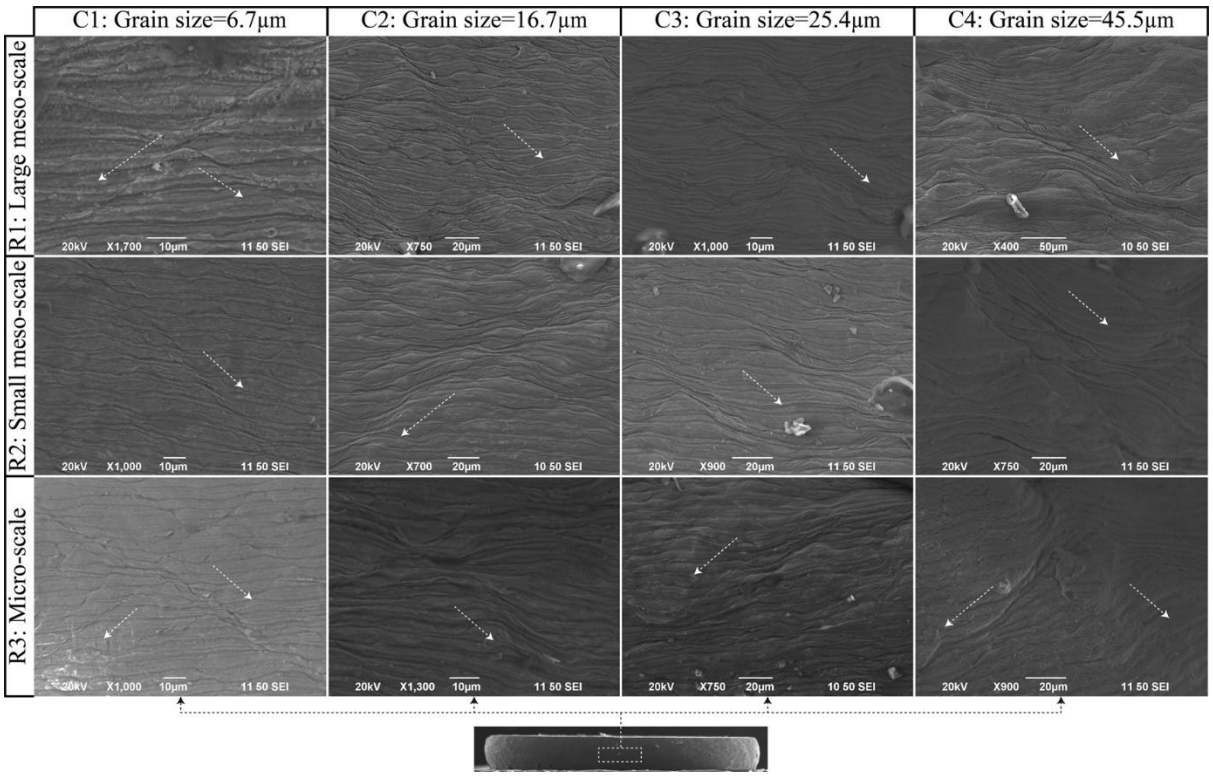

Fig. 9. SEM observation of circumferential surfaces of compression samples.

Fig. 10 shows the microvoids in cross-sectional surface of specimens with different d and geometrical size after compression test. All specimens have a number of microvoids inside but these voids do not connect together and form the macroscopic shear band fracture, which means the failure has happened before the stroke reaches its limit. Failure initiation was associated with micro-cracking due to inclusion in grain boundary or grain boundary itself. In the plastic deformation process inclusion in grain boundary will be broken under the influence of stress. Then this spot will produce stress concentration and thus the micro-void will be generated. These voids may coalesce and grow to form micro-crack. So this uneasily

discovered failure should be drawn more attention, thus the numerical simulation is needed to describe this phenomenon and predict the ductile fracture as precisely as possible.

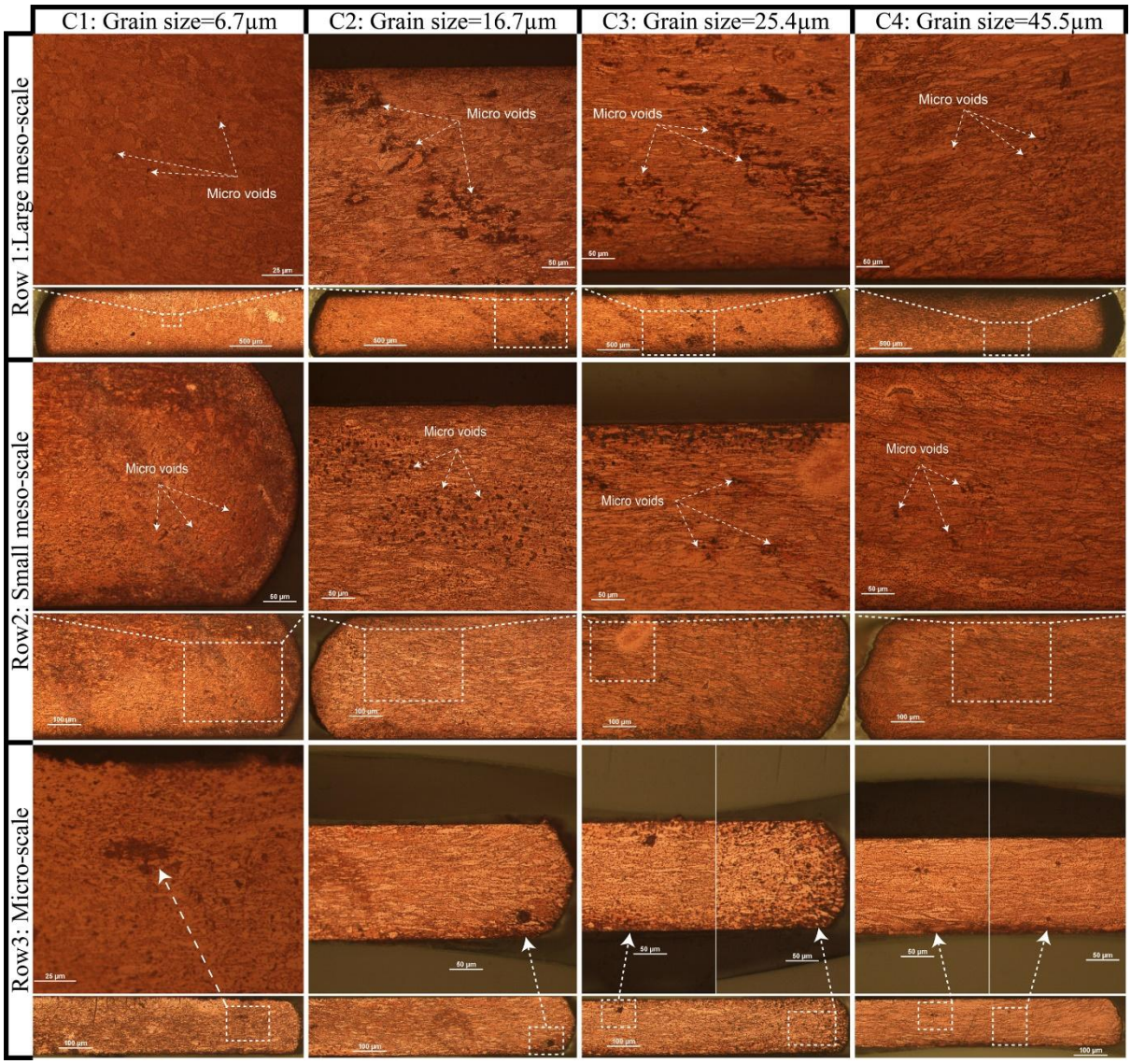

Fig. 10. Cross-sectional photograph of micro voids after compression tests.

For the tensile test the stress stare is different with that of compression. The SEM fractographies of tensile testing samples are shown in Fig. 11. Prior to ductile fracture, localization (necking) occurred in all tensile tests samples. For the large ratio of thickness and grain size these samples are considered as macroscopic polycrystal material, and the fracture surfaces show complex deformation which include many slips and voids. From Fig. 11 Row 3 many enlarged voids and slips locate in the center region of the fracture surface. As

decreasing of η, i.e. the smaller thickness and larger grain size, stress localization tends to locate in several grains boundary, which means the slip of grain is more obvious and the number of micro voids are tapered off in fracture surfaces, as shown in Fig. 11 Row 1 and 2. Even for Row 1 Column 3 and Row 1 Column 4 there are no micro voids, just have slip of grains. This phenomenon is coincident with cross-sectional photographs of fracture position as shown in Fig. 12. When few grains located along the thickness, the property of material is greatly inhomogeneous and the deformation tends to localize in the early stage, thus the uneven deformation behavior occurs, which are quite different from those in macroscopic scenario.

Fig.12 shows cross-sectional photographs of fracture position of uniaxial tensile samples. The shear fracture occurs along an angle of about 45° to the vertical axis. The shear stress plays an important role in the occurrence of fracture. The fractographs clearly show that necking always occurs and shear band gradually reduce to disappear as increase η. From the Fig. 12 Row 1 Column 4, it can be seen that the crack locates on the grain boundary. From this point of view the fracture behavior in μ-scale is different with m-scale. The single grain has greatly influence on ductile fracture.

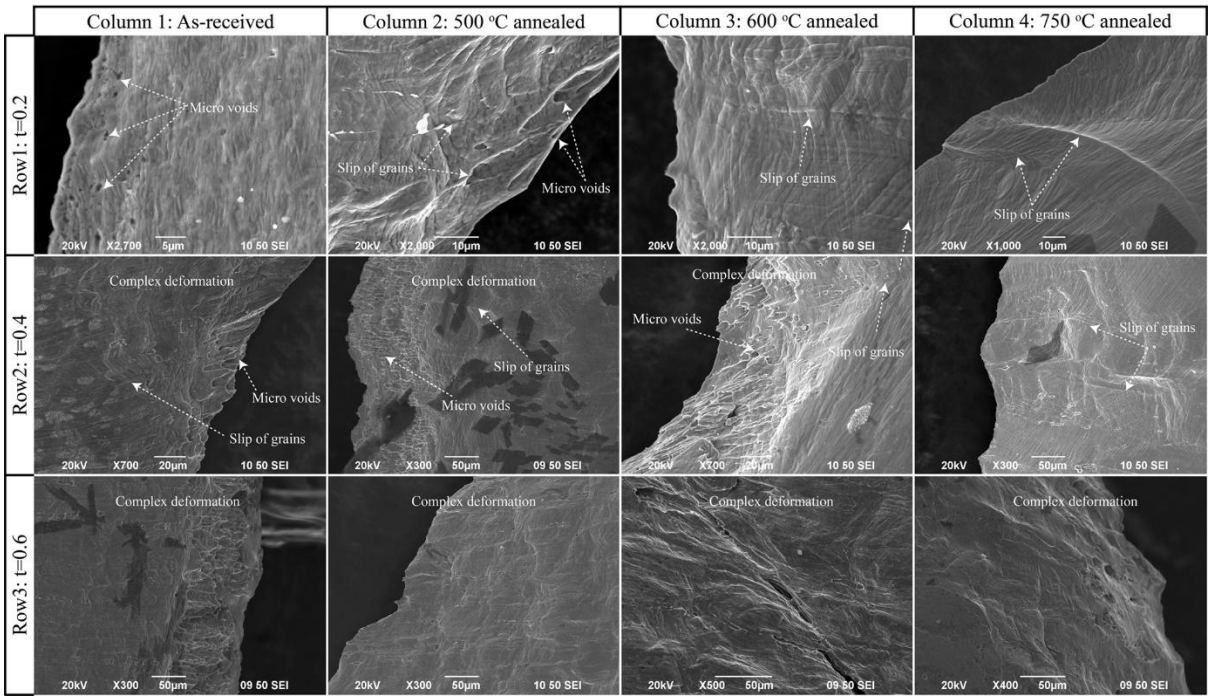

Fig. 11. SEM observation of the fracture surfaces of tensile testing samples.

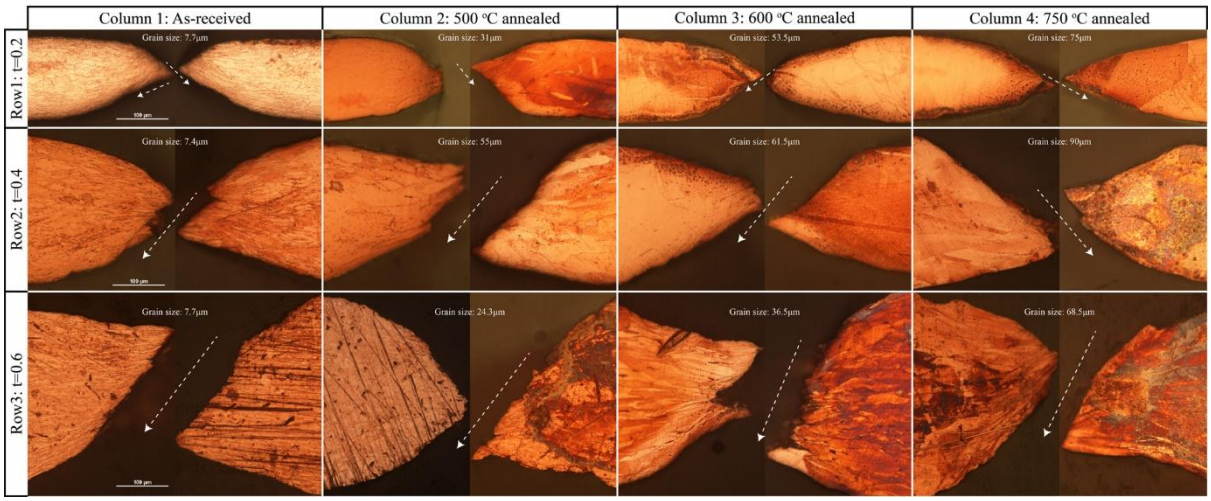

Fig. 12. Cross-sectional photograph of fracture position of uniaxial tensile samples.

4.2. Numerical analysis and discussion

In this research, a commercial FE simulation software-ABAQUS, which is the powerful nonlinear analysis, was used. The parameters needed in material property were all determined

by the SLM and DFCs. As described in Section 3, the stress-strain curves are firstly fitted via small meso-scale compression test and tensile test with t=0.4mm. The flow stress is then calculated according to the ratio of surface grains and grain sizes and inputted as the yield stress in FE simulation. The friction coefficient is also considered based on the frictional correction methods [22, 23] for the compression model. The flow stress cannot represent the material DF property, so the damage energy proposed by Hillerborg et. al [24] needed in damage evolution analysis is determined in the softening part by creating a stress-displacement response. After the fracture strain and damage energy data are inputted into ABAQUS, the final fracture position and data of the multi-scale compression tests and tensile tests can be thus obtained. Fig. 13 (a) shows the initial setting and shear ductile fracture formed after compression in FE simulation. And the initial setting and fracture of tensile specimen are shown in Fig. 13 (b).

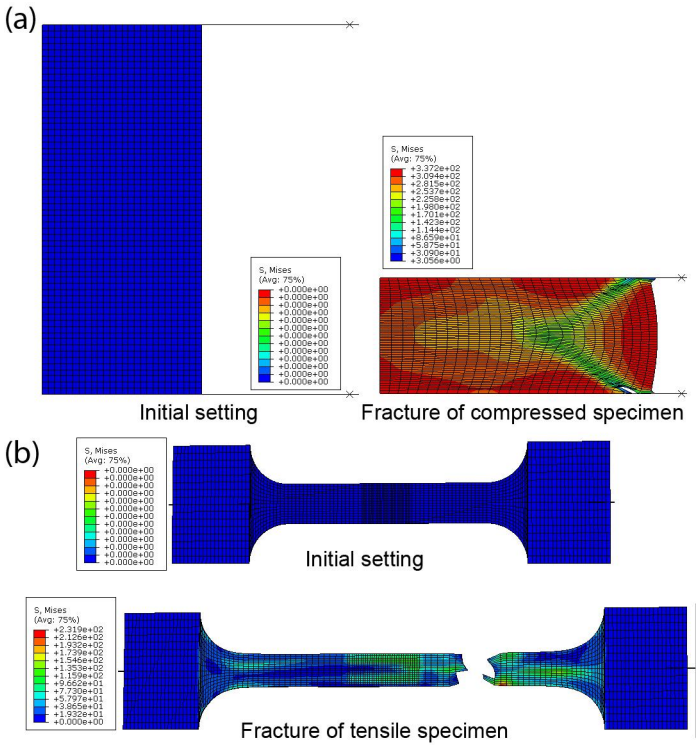

Fig. 13. Simulation model and deformed mesh for (a) compression specimens, and (b) tensile tests.

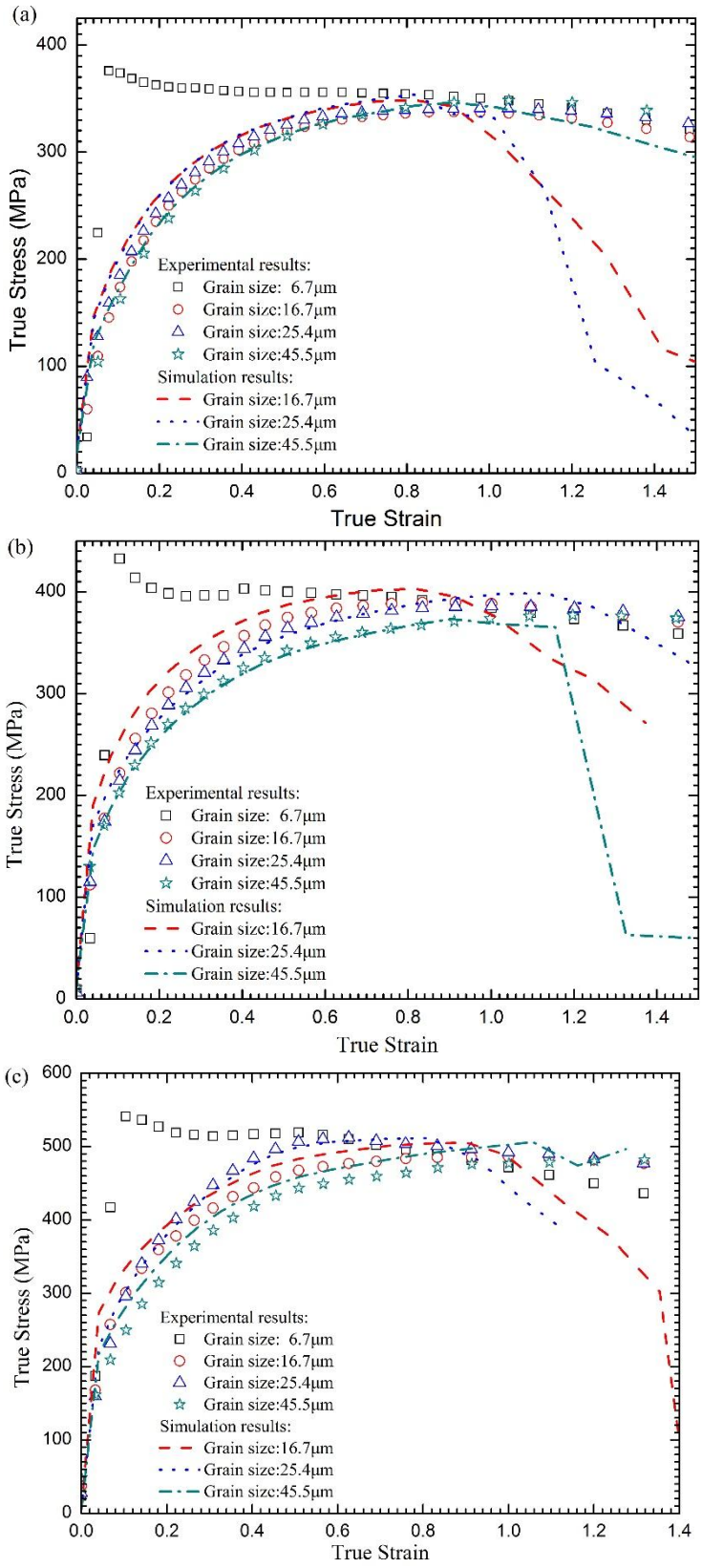

Fig. 14. Comparison of experimental and numerical true stress–strain curves for different *d* in compression tests. (a) Large-meso scale, (b) Small-meso scale, and (c) μ-scale.

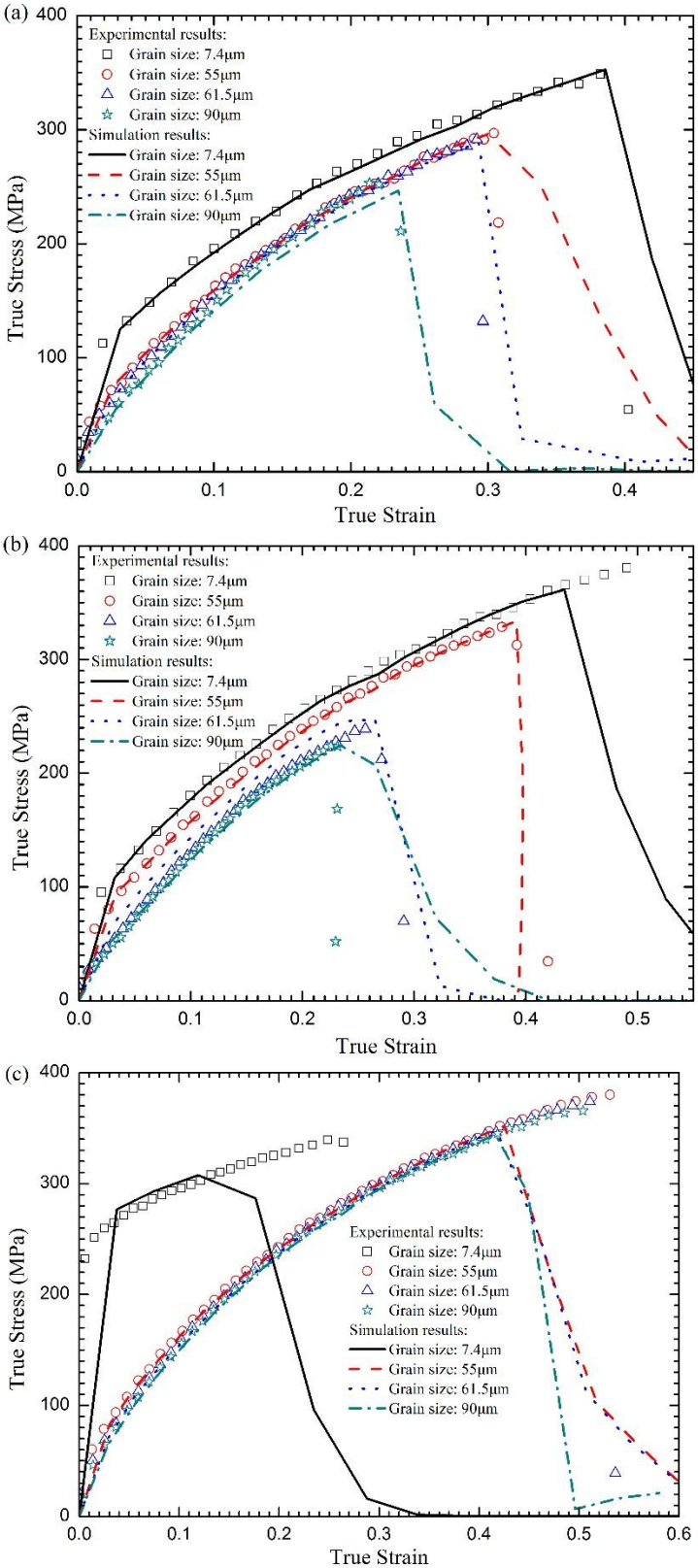

Fig. 15. Comparison of experimental and numerical true stress–strain curves for different *d* in tensile tests. (a) t=0.2, (b) t=0.4, and (c) t=0.6mm.

After FE simulation, stress-strain curves are obtained and also present significant size effects. The simulation results show the excellent agreement with the experiment results. The comparison of experimental and numerical true stress–strain curves for different d in compression tests are shown in Fig.14. For large meso-scale specimens the influence of grain size effect on flow stress is slight due to the small η. As increasing of η the flow stress decrease, which can be seen from Fig.14 (b) and (c). As for the specimen with d=6.7μm (as-received material) the flow stress is greatly affected by foregoing process, which is not suitable for this study. Fig.15 presents the comparison of experimental and numerical true stress–strain curves for different d in tensile tests, which shows the similar tendency with compression tests. More surface grains lead to the smaller flow stress.

4.2.1. Effect of the sizes effect on the fracture stain and energy

Fig. 16 shows the influence of size effects on fracture strain for the compression tests and the tensile tests. The ratio of surface grains indicates the interaction effect of grain size effect and feature size effect. When the ratio of η less than 0.1 the material can be considered as macro polycrystal and fracture strain $\bar{\varepsilon}_f$ are nearly constant under compression stress condition. As increasing of η the fracture strain $\bar{\varepsilon}_f$ shows a change of the sine wave. Although the fracture strain does not have a specific linear relationship with η, under the same feature scale, the d shows an explicit influence on fracture strain. On the large meso-scale case the fracture strain slightly increases with d. For small meso-scale, the fracture strain gradually increase to the maximum at the value of η approximately 0.2. On the μ-scale case the fracture strains show apparent ascending tendency as increasing of d. In other words, η determines the level of influence of d under the same feature size, and the larger η is, the more obvious on grain size effect. But the feature size effect on fracture strain does not show a distinct relationship.

In addition, for large η the fracture strain has a severe scatter due to the fact that anisotropy, d, and orientation of single grain play an important role in an entire specimen.

In the tensile tests, the fracture strains generally decrease with increasing of η and when η less than 0.2 fracture strains are almost the same, which is larger than that in compression tests. The grain sizes show the contrast effects with that in compression tests, which is under the same thickness the fracture strain reduce with increasing of grain size. Moreover, the fracture strains slightly decrease with feature size. But when η is about 0.3, the t=0.4mm case with d=61.5μm and the t=0.2 mm case with d=31μm show different fracture strains, which means that the interaction effect of feature size and grain size can not completely be represented by η. There is maybe a weight relationship between these two effects.

In order to obtain the fracture energy of the deformation material the Freudenthal's criterion [25] is used. So, the fracture energy value can be calculated according to following form:

$$C = \int_0^{\bar{\varepsilon}_f} \sigma\left(\varepsilon\right) d\,\varepsilon \tag{13}$$

In m-scale deformation process, the polycrystal material model is used while in microforming process, the SLM is more accurate compared with the conventional model. Therefore, the fracture energy can be obtained from FE simulation.

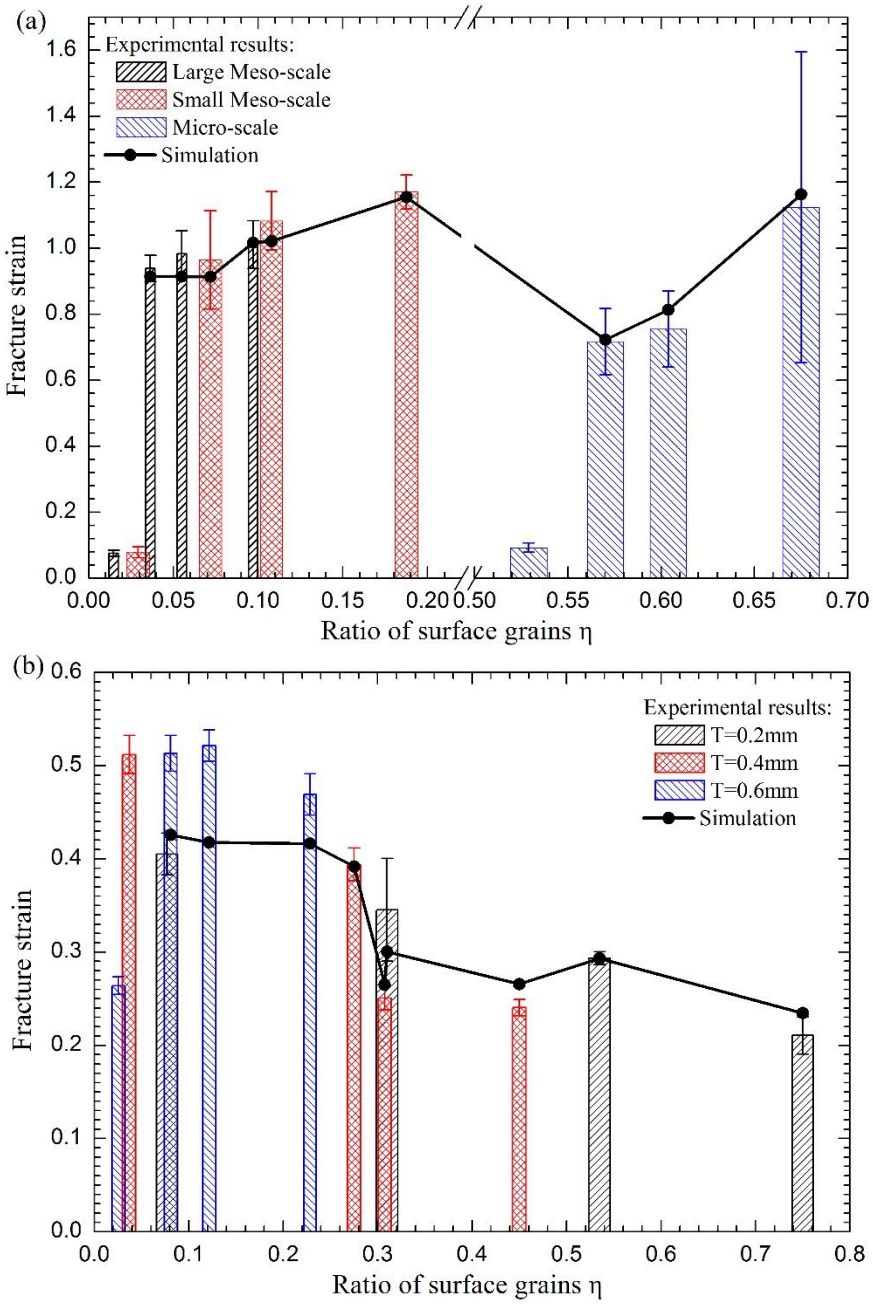

Fig. 16. Comparison of predicted and experimental fracture strain vs. η curves for (a) compression and (b) tensile tests.

Fig.17 shows the influence of size effects on fracture energy for the compression tests and the tensile tests. In the tensile tests, the fracture energy shows the same variation with fracture strain. However, generally, in compression tests the fracture energy steadily rises with η, which means the μ-scaled specimen could undergo more plastic deformation compared to

m-scale specimen. But it is important to realize that severe scatter will affect the precision of results. On the other hand, this scatter could be induced by interaction of anisotropy of grain sizes and interfacial friction.

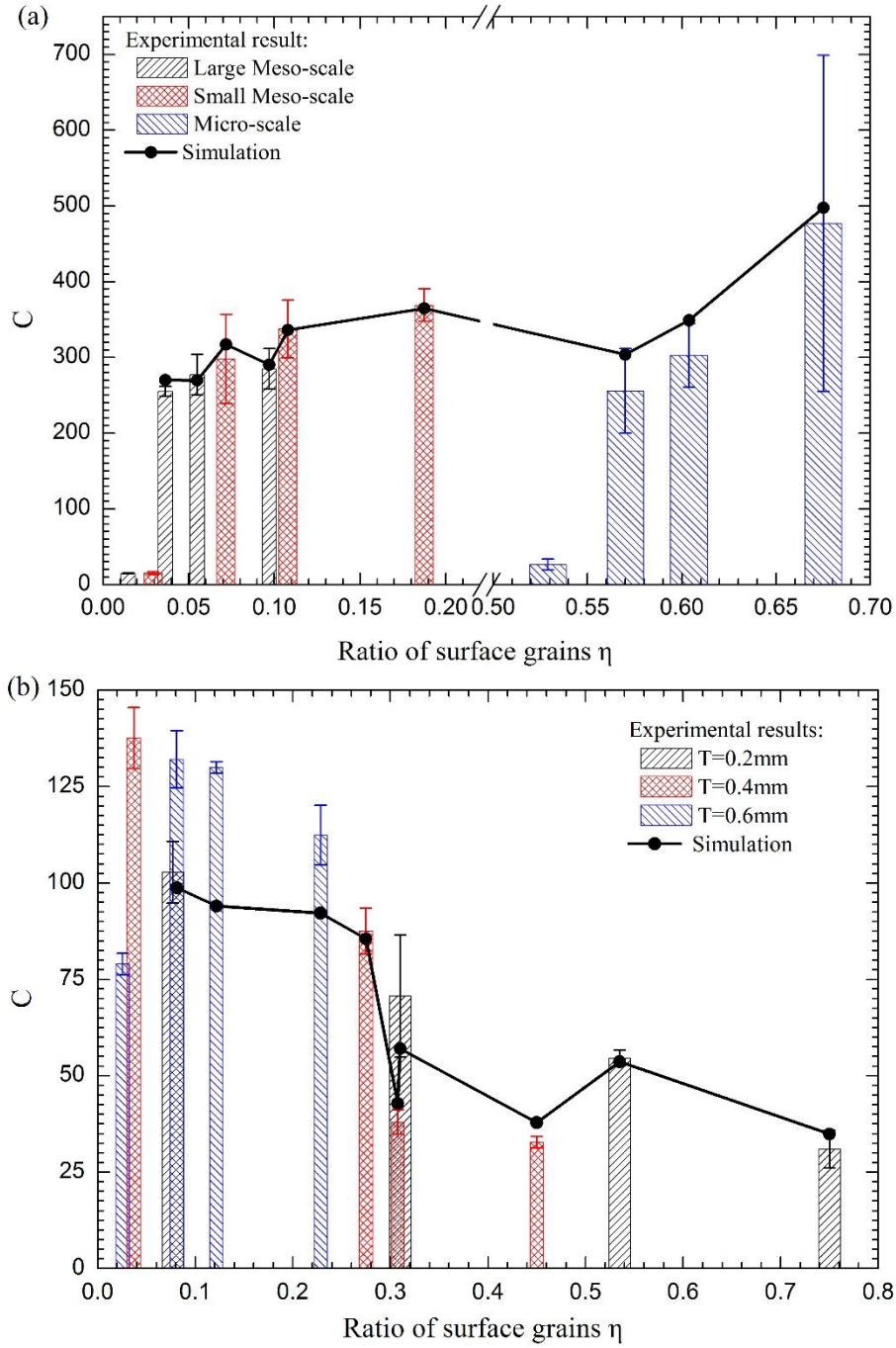

Fig. 17. Comparison of predicted and experimental fracture energy vs. η curves for (a) compression, and (b) tensile tests.

4.2.2. Effect of the stress condition on the fracture strain and energy

The stress triaxiality (T) has relatively slight influence on plasticity but a remarkable influence on DF strain [26]. Fig. 18 shows the T change as η for compression tests obtained from FE simulation. It is found that T overall increases with η, which means the size effects have a significant effect on material fracture and mechanical behavior and also proved that specimen in micro-scale can experience relative large plastic deformation. But for the tensile tests, the T is almost the same regardless of any feature and grain sizes. From this point of view this phenomenon reflects different deformation and fracture mechanisms involved in compression and tensile tests.

The relationship of fracture strain, energy and T are shown in Fig.19. It is clearly seen that the fracture strain and energy with positive T are much smaller than that with negative T no matter what feature and grain sizes. However, the influence of T on fracture strain and energy in negative range are overall consistent with influence of η.

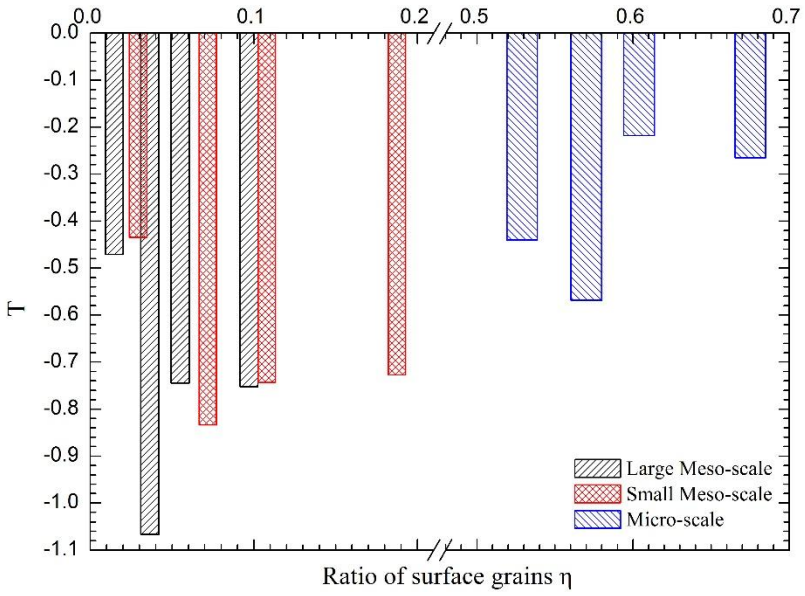

Fig. 18. Stress triaxiality (T) vs ratio of surface grains curves for the compression tests

obtaining from FE simulation.

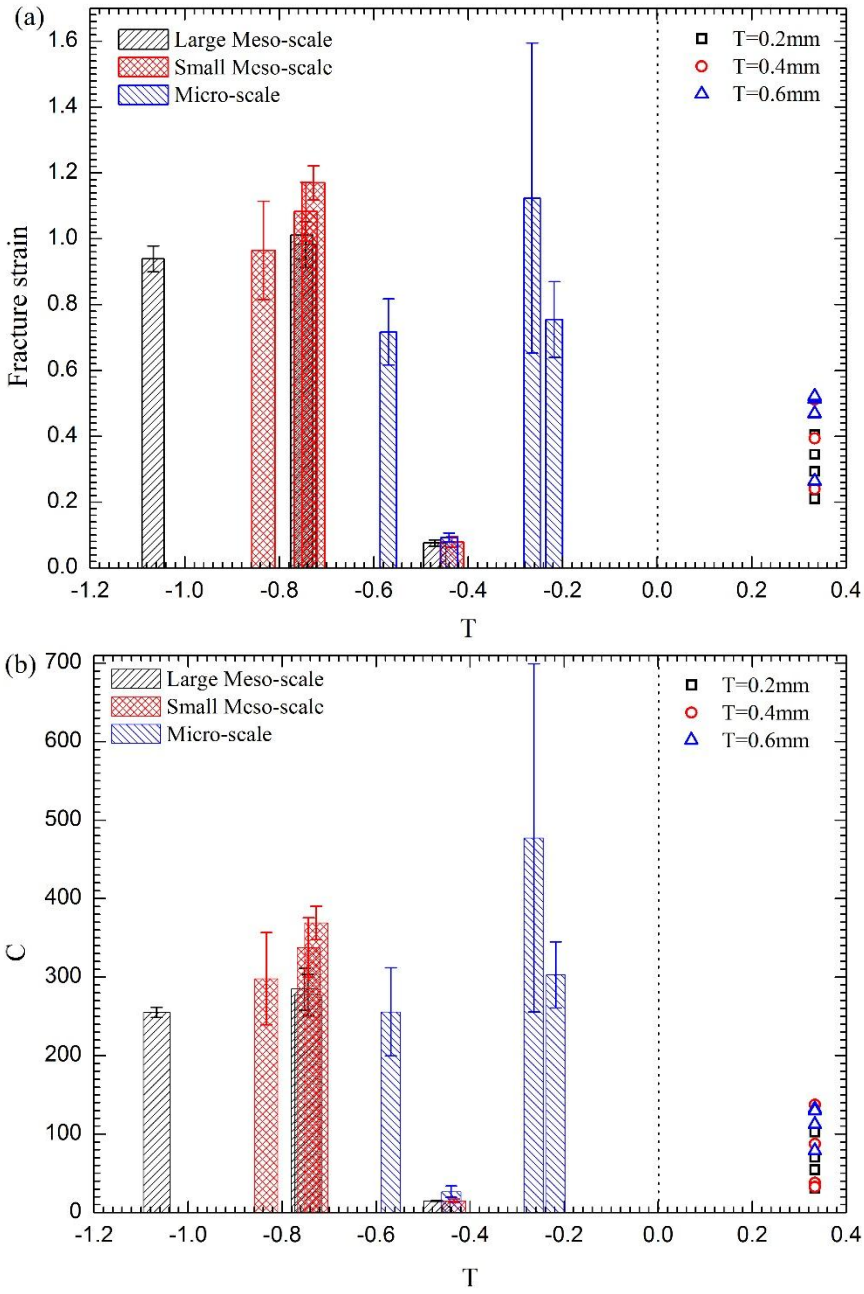

Fig. 19. (a) Fracture strain vs. stress triaxiality (*T*) curves, and (b) Fracture energy vs. stress triaxiality (*T*) curves.

4.3. Application and evaluation of DFC

To further verify these results cup drawing tests using pure copper sheet with *t*=0.2mm were conducted. Fig. 20 shows the designed dimension of cup and fractured sample. Simulation of

the drawing process was performed based on the size effect dependent surface layer model. The simulation results show that the position of fracture is the same with the formed part.

From comparison of load-stroke curve between experiments and simulations presented in Fig. 21, it is clear that the proposed surface layer model has a good agreement with the experimental results. As grain sizes increase the displacement of fracture occurrence decrease, which means the sheet become weaker.

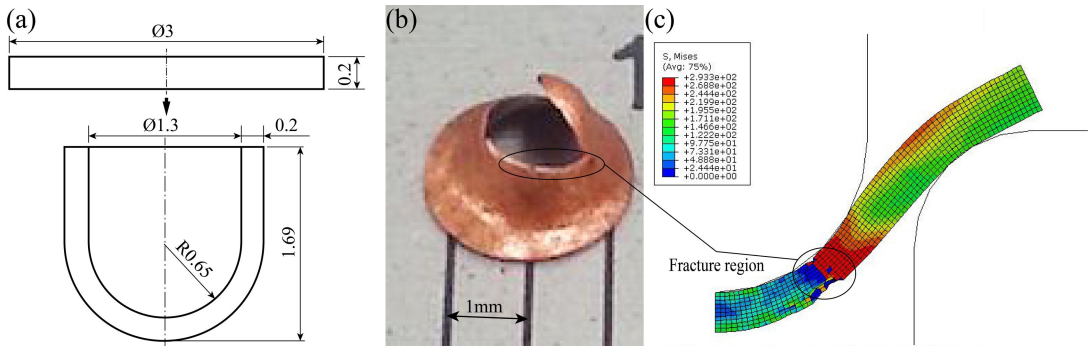

Fig. 20. Cup drawing. (a). Designed dimension, (b). Formed part with fracture, and (c). Fracture region in simulation

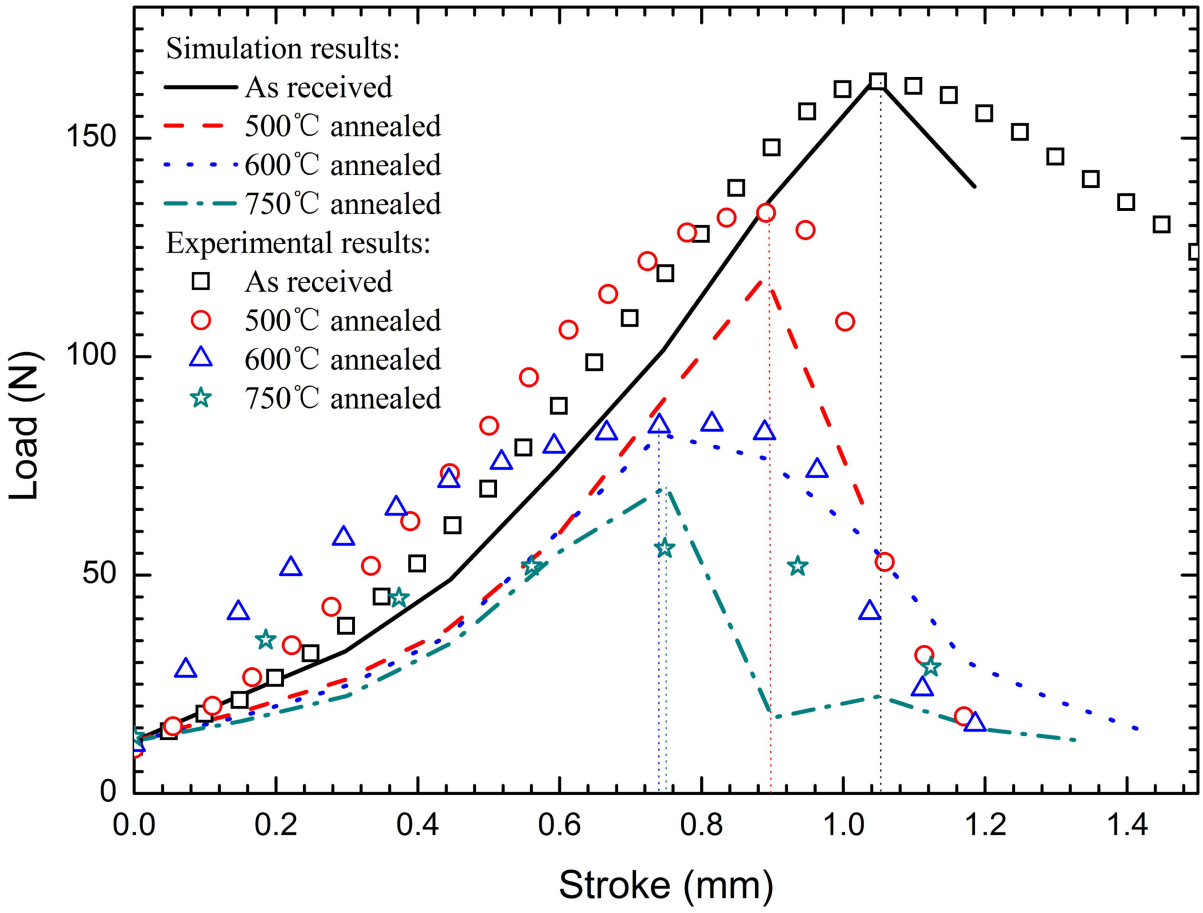

Fig. 21. Comparison of load-stroke curve between experiments and simulations.

5. Conclusions

The influence of size effects and stress condition on DF at multi-scale was investigated by experiments and numerical simulation. The following concluding remarks can be drawn accordingly:

1. Microvoids in cross-sectional surface of specimens after compression test are found, and even though no apparent fracture this voids inside material will destroy strength of material. The fracture strain and the number of microvoids on the fracture surface decrease with *t/d* in tensile tests.

2. The flow stress data determined based on SLM is accurate in dealing with the compression and tensile specimens with different feature and grain sizes.

3. Under the same feature scale the fracture strain and energy increase with grain size in compression test. η determines the level of influence of grain size under the same feature size, and the larger η is, the more obvious on grain size effect.

4. Stress triaxiality (T) generally increases with ratio of surface grains η in compression statement. Fracture strain and energy with positive T are much smaller than that with negative T regardless of feature and grain sizes.

Acknowledgement

The authors would like to thank the funding support to this research from the General Research Fund of Hong Kong Government under the project of 515012 and the projects of G-YBDM, G-YM93, G-U923, and G-UB59 from The Hong Kong Polytechnic University.

Reference

[1] Geiger M, Kleiner M, Eckstein R, Tiesler N, Engel U. Microforming. CIRP Annals - Manufacturing Technology. 2001;50:445-62.

[2] Razali AR, Qin Y. A Review on Micro-manufacturing, Micro-forming and their Key Issues. Procedia Engineer. 2013;53:665-72.

[3] McClintock FA. A criterion for ductile fracture by the growth of holes. Journal of Applied Mechanics. 1968;35:363.

[4] Rice JR, Tracey DM. On the ductile enlargement of voids in triaxial stress fields∗. Journal of the Mechanics and Physics of Solids. 1969;17:201-17.

[5] Gurson AL. Continuum Theory of Ductile Rupture by Void Nucleation and Growth: Part I—Yield Criteria and Flow Rules for Porous Ductile Media. J Eng Mater Technol. 1977;99:2-15.

[6] Cockcroft M, Latham D. Ductility and the workability of metals. J Inst Metals. 1968;96:33-9.

[7] Brozzo P, Deluca B, Rendina R. A new method for the prediction of formability limits in metal sheets. Proc 7th biennal Conf IDDR1972.

[8] Bai YL, Wierzbicki T. A new model of metal plasticity and fracture with pressure and Lode dependence. Int J Plast. 2008;24:1071-96.

[9] Liu HS, Fu MW. Prediction and analysis of ductile fracture in sheet metal forming-Part I: A modified Ayada criterion. Int J Damage Mech. 2014;23:1189-210.

[10] Hambli R, Reszka M. Fracture criteria identification using an inverse technique method and blanking experiment. International journal of mechanical sciences. 2002;44:1349-61.

[11] Li H, Fu M, Lu J, Yang H. Ductile fracture: Experiments and computations. Int J Plast. 2011;27:147-80.

[12] Ran JQ, Fu MW, Chan WL. The influence of size effect on the ductile fracture in micro-scaled plastic deformation. Int J Plast. 2013;41:65-81.

[13] Ran JQ, Fu MW. A hybrid model for analysis of ductile fracture in micro-scaled plastic deformation of multiphase alloys. Int J Plast. 2014;61:1-16.

[14] Meng B, Fu MW. Size effect on deformation behavior and ductile fracture in microforming of pure copper sheets considering free surface roughening. Mater Design. 2015;83:400-12.

[15] Engel U, Eckstein R. Microforming - from basic research to its realization. J Mater Process Technol. 2002;125:35-44.

[16] Peng L, Lai X, Lee H-J, Song J-H, Ni J. Analysis of micro/mesoscale sheet forming process with uniform size dependent material constitutive model. Mater Sci Eng, A. 2009;526:93-9.

[17] Lai X, Peng L, Hu P, Lan S, Ni J. Material behavior modelling in micro/meso-scale forming process with considering size/scale effects. Comput Mater Sci. 2008;43:1003-9.

[18] Armstrong R, Codd I, Douthwaite R, Petch N. The plastic deformation of polycrystalline aggregates. Philos Mag. 1962;7:45-58.

[19] Armstrong R. The yield and flow stress dependence on polycrystal grain size. Yield, flow and fracture of polycrystals. 1982:1-31.

[20] Mecking H, Kocks U. Kinetics of flow and strain-hardening. Acta Metall. 1981;29:1865-75.

[21] Clausen B, Lorentzen T, Leffers T. Self-consistent modelling of the plastic deformation of fcc polycrystals and its implications for diffraction measurements of internal stresses. Acta Mater. 1998;46:3087-98.
[22] Wanjara P, Jahazi M, Monajati H, Yue S, Immarigeon J-P. Hot working behavior of near-α alloy IMI834. Mater Sci Eng, A. 2005;396:50-60.
[23] Ebrahimi R, Najafizadeh A. A new method for evaluation of friction in bulk metal forming. J Mater Process Technol. 2004;152:136-43.
[24] Hillerborg A, Modéer M, Petersson P-E. Analysis of crack formation and crack growth in concrete by means of fracture mechanics and finite elements. Cem Concr Res. 1976;6:773-81.
[25] Freudenthal A. The inelastic behavior of solids. Wiley, New York. 1950.
[26] Gao XS, Zhang TT, Hayden M, Roe C. Effects of the stress state on plasticity and ductile failure of an aluminum 5083 alloy. Int J Plast. 2009;25:2366-82.